A DETAILED STUDY TOWARD THE NANO -CRYSTALLIZATION OF α – Fe IN $Fe_{55-X}Cr_{18}Mo_7B_{16}C_4$ BULK AMORPHOUS ALLOY

S. Ahmadi[1] and H. R. Shahverdi[2]

* *sh.ahmadi@modares.ac.ir*

Received: November 2014 **Accepted: April 2015**

[1] Materials and Biomaterials Research Center, Biomaterials Group, Tehran, Iran.

[2] Faculty of Engineering, Department of Materials Science, Tarbiat Modares University, Tehran, Iran.

Abstract: *Crystallization of α – Fe phase during annealing process of Fe55Cr18Mo7B16C4 bulk amorphous alloy has been evaluated by X- ray diffraction, differential scanning calorimetric tests and TEM observations in this research. In effect, crystallization mechanism and activation energy of crystallization were evaluated using DSC tests in four different heating rates (10, 20, 30, 40 K/min). A two -step crystallization process was observed in the alloy in which α–Fe phases was crystallized in the first step after annealing process. Activation energy for the first step of crystallization process (i.e. α – Fe phase) was measured to be 276 (Kj/mole) according to Kissinger kinetic model. Furthermore, Avrami exponent calculated from DSC curves was two and a three -dimensional diffusion controlled mechanism with decreasing nucleation rate was observed in the alloy. It is also known from the TEM observations that crystalline α – Fe phase nucleated in the structure of the alloy in an average size of 10 nm and completely mottled morphology.*

Keywords: *Bulk Metallic Glasses (BMGs); Kissinger model; morphology; Crystallization*

1. INTRODUCTION

Bulk metallic glasses or bulk amorphous alloys, named as one of the newest synthetic structural materials, have been attracted much attention in two last decades due to their unique properties [1-3]. In particular, formation of nanosize crystals during annealing process was mentioned as one of the most striking features of the materials. In fact, it is proof that unstable amorphous (or glassy) structures can be devitrified to the stable nanostructures composed of nanosize crystals by heat treating over the crystallization temperatures [4].

Generally, nucleation of crystalline phases during heat treatment and formation of nanostructure alloys have been studied by two main ways: (i) kinetic evaluations in isothermal or non- isothermal methods and (ii) microstructural evaluations by TEM or STEM [5, 6].

Crystallization process has been characterized in some kinds of Fe- base bulk metal glasses by D. j. Branagan and his coworkers [7, 8]. Microstructural evaluation in these kinds of BAMs showed that complex carbides (e.g. $Fe_{23}(B, C)_6$ and some phases such as Fe_3B and Fe_2B were nucleated into the amorphous structures after annealing process. It was also known that not only hardness and wear resistance of the alloys were promoted effectively but also abrasion and fretting resistance were also enhanced drastically by nucleating of nanosize phases [9, 10].

Kinetics of crystallization process in amorphous alloys has been evaluated using calorimetric tests and kinetic models such as Kissinger- starink, Ozawa, and Matusita. All these models were categorized in non- isothermal analysis of crystallization in metallic glasses. Activation energy of crystallization, Avrami exponent, and growth mechanisms can be investigated using these models. In practice, characterization of crystallization process in Fe-base magnetic amorphous alloys such as $(Fe_{50}Co_{50})_{73.5}Ag_1Nb_3Si_{13.5}B_9$, $Fe_{83}B_{17}$ and $Fe_{75}Si_9B_{16}$ has been showed a diffusion controlled growth mechanism and two step crystallization process in the alloys [11-13].

In this research work, for the first time, crystallization kinetics of $Fe_{55}Cr_{18}Mo_7B_{16}C_4$ bulk amorphous alloy were evaluated using X- ray diffraction, DSC tests, and TEM observations. In fact, activation energy and types of crystallized phases were investigated during crystallization of

[DOI: 10.22068/ijmse.12.2.83]

the alloy. Experimental

Multi- component Fe- based alloy ingots were prepared in an arc furnace with nominal compositions of $Fe_{55}Cr_{18}Mo_7B_{16}C_4$. Pure iron (99.7 mass %), chromium (99.9 mass %), molybdenum (99.9 mass %), and crystalline boron (99.5 mass %) were used to produce ingots in a rod form. To achieve fully amorphous structures, rapidly solidified thin ribbons with a thickness of about 60 μm were prepared by melt-spinning technique (wheel speed: 32 m/s). Then, amorphous ribbons were annealed under vacuum (10-3 torr) in a furnace above their crystallization temperatures. X- ray diffraction (XRD) with Cu Kα radiation and differential scanning calorimetric (DSC) tests, at four different heating rates, were used to determine the crystalline phases and transformation temperatures. Argon was used as both a purge and protective gas during DSC test. Base-lines in differential scanning calorimetric tests were determined by not using any sample at all or using "empty pan" method.

Composition of the ribbons was verified by using energy- dispersive X-ray spectroscopy. A 200 kV JEOL transmission electron microscope equipped with an energy dispersive X-ray spectrometer (INCA PentaFETx$_3$ - Oxford instruments) was used to microstructural evaluations. Before applying microstructural determination, samples were prepared in foil shape with 3mm diameter. These discs were electro-polished in twin jet electro-polisher with a solution composed of nitric acid.

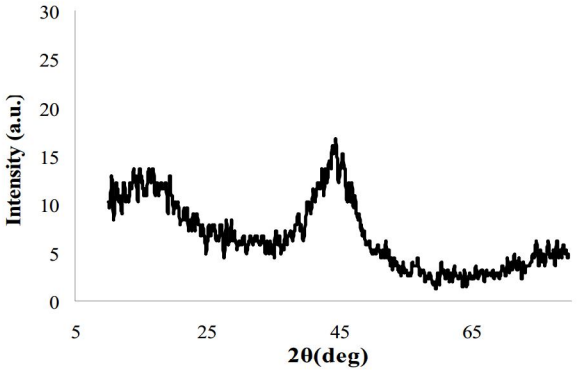

Fig. 1. XRD pattern of $Fe_{55}Cr_{18}Mo_7B_{16}C_4$ in amorphous state.

2. RESULTS AND DISCUSSION

2.1. Crystallization of α – Fe Phase

In Figure 1, XRD pattern of $Fe_{55}Cr_{18}Mo_7B_{16}C_4$ alloy (after melt-spinning process) is shown demonstrating a broad amorphous scattering peak. No peaks corresponding with crystalline phases are showed which means fully amorphous structure was formed in the sample after melt-spinning process.

In addition, the amorphous steel alloy was scanned in DSC test at 10, 20, 30, and 40 K/min heating rates (Fig. 2). Two peaks were observed in all thermo-grams showing two -stage crystallization process in the alloy. It is seen that

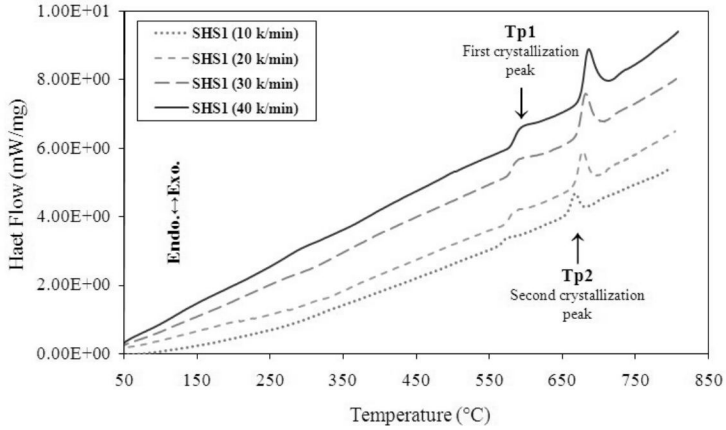

Fig. 2. DSC thermograms of the alloy at four different heating rates.

[DOI: 10.22068/ijmse.12.2.83]

Table 1. Changes of the first crystallization temperature (i.e. α–Fe crystallization) in the alloy

Alloy	*Heating Rate*	*10 K/min*	*20 K/min*	*30 K/min*	*40 K/min*
$Fe_{55}Cr_{18}Mo_7B_{16}C_4$	T_{P1} (°C)	575	589	593	597

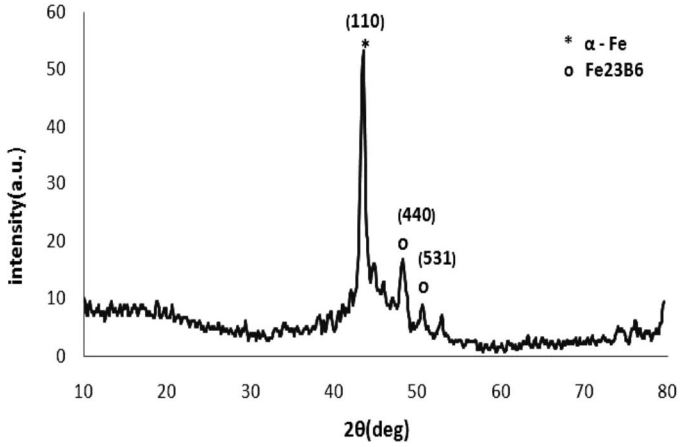

Fig. 3. XRD pattern of $Fe_{55}Cr_{18}Mo_7B_{16}C_4$ alloy annealed at 650°C / 3 h.

the peak temperatures increase with increasing heating rate and this suggests that the crystallization should be classified in the temperature dependent and diffusion controlled transformations. In Table 1, changes in the first (T_{P1}) crystallization peak with increasing heating rate in $Fe_{55}Cr_{18}Mo_7B_{16}C_4$ alloy are given.

To characterize the types of the crystallized phases, amorphous ribbons were annealed. In effect, temperature was chosen above the first crystallization temperature. Figure 3 shows the XRD pattern of the crystallized ribbons. It is clear from Figure 3 that α - Fe and $Fe_{23}B_6$ phases were crystallized respectively in the structure after annealing process. In general, crystallization of α–Fe, $Fe_{23}C_6$, and Fe_3B phases in Fe-based bulk amorphous steels was reported by D. J. Branagan [8-10].

2.2. Activation Energy of Crystallization

Kissinger- Starink peak method (equation 1) was effectively used in this research to investigate the activation energy, Ea, in the first step of crystallization (i.e. α – Fe) phase in the alloys.

According to the equation 1, Kissinger-Starink model, plotting ln (β /T_{P2}) versus 1/T_P gives a straight line and slope of it equals to -Ea/R [14].

$$\ln \frac{\beta}{T_P^2} = -\frac{E_a}{RT_P} + C \qquad (1$$

Where β is heating rate, R is the gas constant, and T_P is the peak temperature.

Arrhenius plot derived from Kissinger- Starink model for the first endothermic heat effect in the alloy is shown in Figure 4. Activation energy for crystallization of α–Fe phase in the $Fe_{55}Cr_{18}Mo_7B_{16}C_4$ alloy was measured to be 276 (Kj/mol). In comparison with other diffusion controlled solid state transformations such as precipitation hardening, high value of activation energy in crystallization of the amorphous alloy can be attributed to mass displacement of atoms. In other words, activation energy can be spent not only to overcome the energy barrier required to diffusion of atoms but also to nucleation and

[DOI: 10.22068/ijmse.12.2.83]

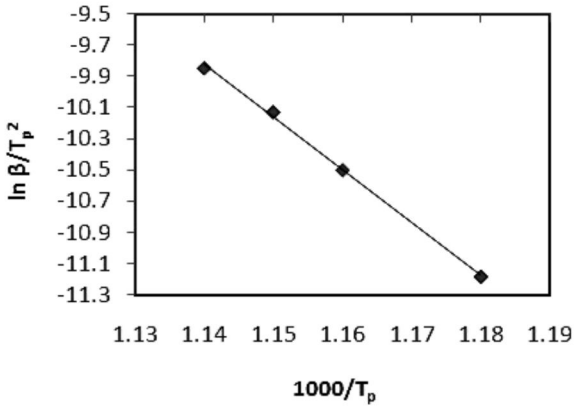

Fig. 4. Arrhenius plot for crystallization of α – Fe phase in $Fe_{55}Cr_{18}Mo_7B_{16}C_4$ alloy.

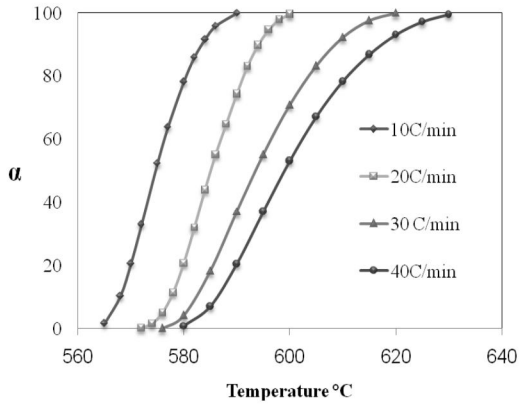

Fig. 5. Fraction of crystallization (α) as a function of temperature at four different heating rates in $Fe_{55}Cr_{18}Mo_7B_{16}C_4$ alloy.

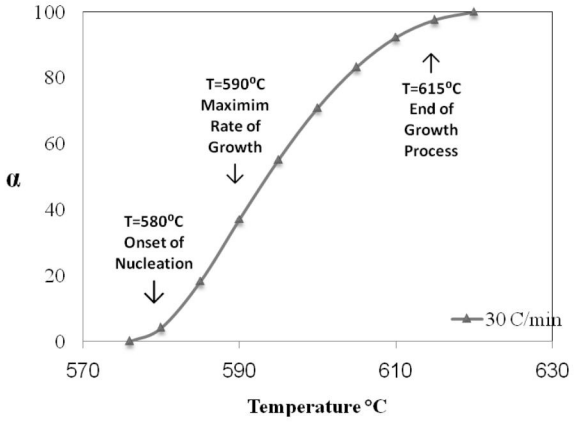

Fig. 6. Temperatures showing onset of nucleation, subsequent crystallization, and growth processes of α-Fe in $Fe_{55}Cr_{18}Mo_7B_{16}C_4$ alloy with respect to calorimetric tests and chart of transformed volume fraction- α.

growth of nanocrystalline phases. Specifically, activation energy in this research work was related to mass displacement of atoms in which α–Fe crystalline phase formed in the structure after annealing process.

The volume fraction of transformed structure from amorphous to crystalline state (or degree of devitrification) can be derived from DSC thermograms as a function of temperature. At each temperature, volume fraction of crystallization (α) is given according to equation 2 [15].

$$\alpha = S_i / S_T \quad (2$$

Where S_T is the total area of the exothermic peak and S_i is the area among initial point of the peak and any other temperature. In Figure 5 the plot of α versus temperature is shown for the first step of crystallization (α–Fe) in the alloy.

It can be seen clearly, the most striking feature of the chart is the sigmoid shape of it. In some other researches [15, 16] these kinds of fraction curves were interpreted to diffusion controlled and dimensional growth mechanisms (two or three) during crystallization. It is proof that the temperatures of the onset of nucleation and maximum rate of growth can be investigated from DSC thermograms [15]. In Figure 6 these mentioned temperatures is shown for the alloy.

2.3. TEM Observations

One of the most striking features of the nanostructured Fe based alloys produced by annealing a preliminary amorphous state is the distinct appearance / morphology of the crystalline phases. For example crystalline α - Fe in the alloys form a mottled structure; the $Fe_{23}C_6$ phase forms a featureless smooth structure [17]. In Fig. 7 microstructure of the primary alloy in amorphous state is shown. Specifically, no crystalline phases are detected in the figure.

In Fig. 8 microstructure of the crystalline alloy after heat treatment is shown. It is clear from the images that crystalline α–Fe is nucleated in the amorphous structure after annealing. Indeed, complex or partly crystalline structure formed due to heat treatment above the first crystalline temperature.

[DOI: 10.22068/ijmse.12.2.83]

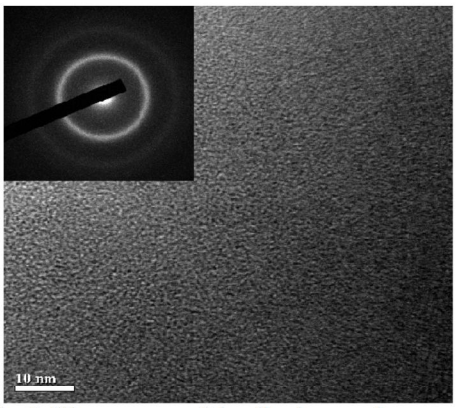

Fig. 7. Microstructure of the alloy in amorphous state.

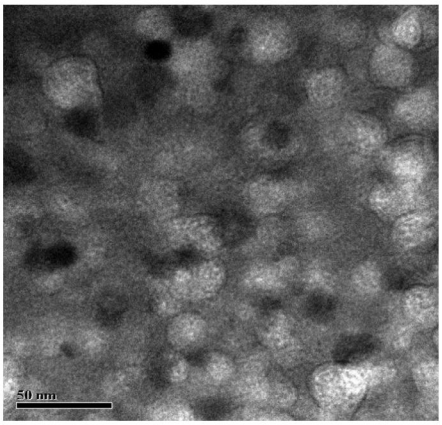

Fig. 8. Microstructure of the alloy in crystalline state STEM image.

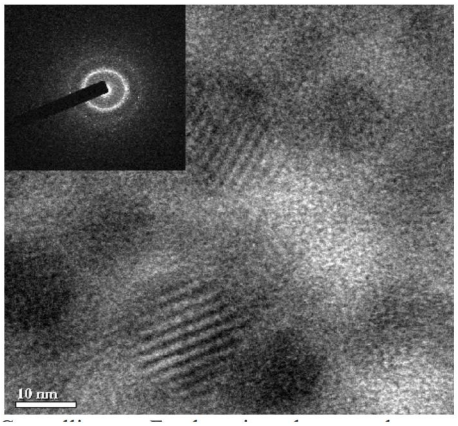

Fig. 9. Crystalline α – Fe phase into the amorphous structure.

Size and morphology of α–Fe crystalline phases are showed in Fig. 9. As mentioned above, unique feature of the crystalline phases in structure of the nanostructure Fe base alloys can be effectively used toward identification of these nanosize phases. As can be seen clearly from the Figure 9, crystalline α–Fe phase nucleated in the structure an average size of ten nm and completely mottled morphology.

2. 4. Growth Mechanism in Crystallization of the Alloy

To show the exact mechanisms of growth in the alloy, Matusita model was used (equation 3).

$$\ln [-\ln (1-\alpha)] = -n \ln (\beta) - 1.052(mE_a/RT) + \text{constant} \quad (3)$$

Where α is the volume fraction of crystallization, β is heating rate, E_a activation energy, n is Avrami exponent , m is dimensionality of growth, and R is the gas constant. In this research, by plotting ln [-ln (1-α)] versus ln β at constant temperature Avrami exponent was estimated. Further, by plotting ln [-ln (1-α)] versus temperature (T) at constant heating rate (β) dimensionality growth guideline (m) was derived. In Figures 10 and 11 variation of ln [-ln (1-α)] versus ln β at constant temperature and variation of ln [-ln (1-α)] versus temperature (T) at constant heating rate (β) are shown respectively.

Matusita model differs with Kissinger- Starink method in that it provides useful information about the Avrami exponent and dimension of growth in devitrification of amorphous alloys. In general, Avrami exponent (n) can be estimated according to equation 4 [18].

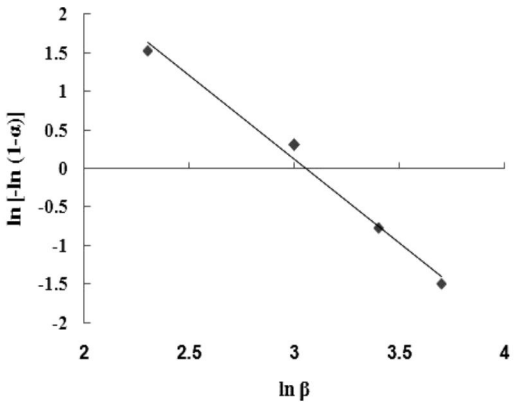

Fig. 10. Ln [-ln (1-α)] as a function of heating rate in constant temperature (T=590°C).

[DOI: 10.22068/ijmse.12.2.83]

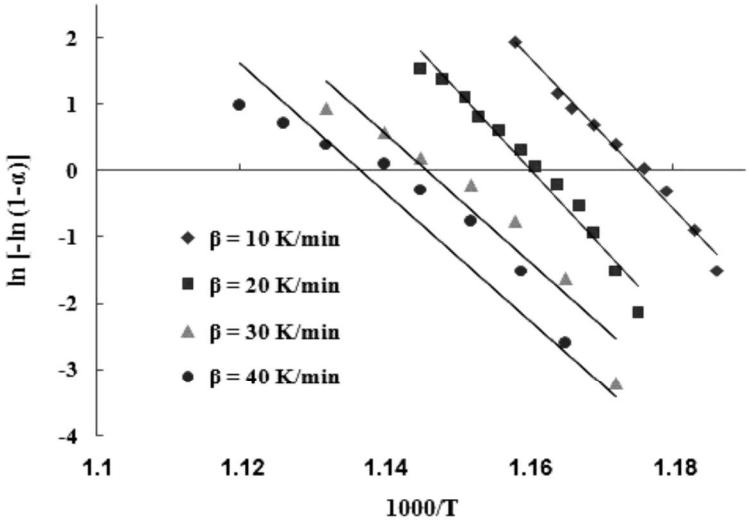

Fig. 11. Matusita plots at different temperatures and constant heating rate.

Table 2. Explanation of nucleation and growth parameters [16, 18]

Parameter	*Amount*	*Explanation*
m	1	One- dimensional growth mechanism
	2	Two- dimensional growth mechanism
	3	Three- dimensional growth mechanism
p	1	Linear growth (interfacial control)
	0.5	Parabolic growth (diffusion control)
b	>1	Increasing nucleation rate
	0	No nucleation during crystallization (this means that all nuclei may be present before devitrification)
	<1	Decreasing nucleation rate

$$n=b+pm \quad (4$$

Where n is Avrami exponent, m is dimensionality growth guideline, b is a guideline showing nucleation rate, and p is a guideline showing type of transformation, e.g., diffusion controlled transformations. In table 2 explanations of these guidelines are given. The amount of Avrami exponent (n) in this research was calculated to be two by considering the slop of the straight line in Fig. 10.

In this research, the average of dimensionality growth guideline (m= 3) can be implied from the slops of straight lines in Fig. 11. In fact, it is though that devitrification process in $Fe_{55}Cr_{18}Mo_7B_{16}C_4$ was carried out by a bulk crystallization mechanism in three dimensions. By considering the growth guidelines in table 2, a diffusion controlled growth mechanism was accomplished in the alloy and thus, the amount of p was considered equal to 0.5. In addition, it is hypothesized that a decreasing nucleation rate (b) was also accomplished in crystallization of $Fe_{55}Cr_{18}Mo_7B_{16}C_4$ alloy resulted from equation four and the amounts of n, m, and p (2, 3, and 0.5 respectively).

[DOI: 10.22068/ijmse.12.2.83]

3. CONCLUSIONS

1. A two- step crystallization process was observed in $Fe_{55}Cr_{18}Mo_7B_{16}C_4$ alloy in which α – Fe phase was crystallized in the first step of crystallization after annealing process.
2. Activation energy for the crystallization of the phase α - Fe was measured to be 276 (Kj/mol) according to Kissinger- Starink model respectively.
3. Crystalline α – Fe phase nucleated in the structure of heat treated $Fe_{55}Cr_{18}Mo_7B_{16}C_4$ alloy in an average size of 10 nm and completely mottled morphology.
4. It is suggested that α - Fe crystals in the structure of the alloy according to a bulk crystallization, diffusion controlled, and dimensional growth mechanism. Indeed, a three -dimensional diffusion controlled growth mechanism and decreasing nucleation rate was found in crystallization of $Fe_{55}Cr_{18}Mo_7B_{16}C_4$ alloy.

ACKNOWLEDGMENT

The authors are grateful to Ms. Mohamadinasab (Iranian Minister Processing Research Center) for kindly help toward accomplishing DSC tests.

REFERENCES

1. Branagan, D. J. and Tang, Y., “Developing Extreme hardness in Iron based Nanocomposite”, Composites, PartA, Vol.33, 2002, 855-859.
2. Inoue, A., Shen, B. L., Koshiba, H., Kato, H., Yavari, A. R., “Ultra-high strength above 5000 MPa and soft magnetic properties of Co–Fe–Ta–B bulk glassy alloys”, Acta Mater. 52, 2004, 1631-1637.
3. Pang, S. J., Zhang, T., Asami, K., Inoue, A., “Bulk glassy Fe–Cr–Mo–C–B alloys with high corrosion resistance”, Corrosion Science, 44, 2002, 1847-1856.
4. Ahmadi, S., Shahverdi, H. R., “Nanocrystallization Mechanisms of $Fe_{52}Cr_{18}Mo_7B_{16}C_4Nb_3$ Bulk Amorphous Steel”, Iranian Journal of Mater. Sci. Eng., Vol. 10, Number 4, 2013, 1-7.
5. Nishiyama, N., and Inoue, A., "Supercooling Investigation and Critical Cooling Rate for Glass Formation in Pd-Cu-Ni-P Alloy', Acta Materialia, No.5, 1999, 1487-1495.
6. Ahmadi, S., Shahverdi, H. R. and Saremi, S. S., “Nano crystallization of α -Fe Crystals in $Fe_{52}Cr_{18}Mo_7B_{16}C_4Nb_3$Bulk Amorphous Alloy ", Journal of Mater. Sci. Eng., 2011, 27(6), 497-502.
7. Ahmadi, S., Shahverdi, H. R. and Saremi, S. S., “Investigation of the Effects of Nb Alloying on Crystallization Kinetics of $Fe_{55-x}Cr_{18}Mo_7B_{16}C_4Nb_x$(X= 0, 3) Bulk Amorphous Alloys”, Journal of Mater. Sci. Eng., 2011, 27(8), 735-740.
8. Branagan, D. J., Marshall, M. C., Meacham, B. E., “High toughness high hardness iron based PTAW weld materials”, Materials Science and Engineering A, Vol.428, 2006, 116–123.
9. Ahmadi, S., Shahverdi, H. R., Afsari, M., Abdollah-zadeh, A., “Nano-Crystallization of $Fe_{36}Cr_{12}Mo_{10}$ Phase in $Fe_{55-x}Cr_{18}Mo_7B_{16}C_4Nb_x$ (X=0, 3, 4) Amorphous alloys ", Journal of Non-cry. Solids, 365, 2013, 47–52.
10. Branagan, D. J., Breitsameter, M., Meacham, B. E. and Belashchenko, V., "High-Performance Nanoscale Composite Coatings for Boiler Applications", Journal of Thermal Spray Technology, ASM International, Volume 14(2), 2005, 196-204.
11. Soliman, A. A., Al-Heniti, S., Al-Hajry, A., Al-Assiri, M., Al-Barakati, G., “Crystallization kinetics of melt-spun Fe83B17 metallic glass”, Thermochimica Acta, Vol.413, 2004, 57–62.
12. Chrissafis, K., Maragakis, M. I., Efthimiadis, K. G., Polychroniadis, E. K., “Detailed study of the crystallization behavior of the metallic glass $Fe_{75}Si_9B_{16}$”, Alloys and Compounds, 386, 2005, 165-173.
13. Ribeiro, R. M., De Biasi, R. S., Dos Santos, D. R., Dos Santos, D. S., “Nano-crystallization of Fe-based amorphous metallic alloys studied by non-isothermal and isothermal techniques”, Journal of Alloys and Compounds, Vol.483, 2009, 495–498.
14. Starink, M. J., “Analysis of aluminum based alloys by calorimetry: quantitative analysis of

[DOI: 10.22068/ijmse.12.2.83]

reactions and reaction kinetics", International Materials Review, 49, 2004, 191-226.

15. Ahmadi, S., Arabi, H., Shokuhfar, A., "Formation Mechanisms of Precipitates in an Al- Cu- Li- Zr Alloy and their Effects on Strength and Electrical Resistance of the Alloy", Journal of Alloys & compounds, 484, 2009.
16. Pratap, A., Lada, K. N., Shanker Raob, T. L., Majmudara, P., Saxenac, N. S., "Kinetics of crystallization of amorphous $Cu_{50}Ti_{50}$ alloy", Journal of Non-Crystalline Solids, Vol. 345&346, 2004, 178–181.
17. Ahmadi, S., Shahverdi, H. R. and Saremi, S. S., "An Investigation toward the Nano-Crystallization of $Fe_{55}Cr_{18}Mo_7B_{16}C_4$ Bulk Amorphous Alloy", Advanced Materials Research, Vols. 383-390 (2012) p p 3858-3862.
18. Ahmadi, S., Shahverdi, H. R. and Saremi, S. S., "Kinetics of α-Fe Crystallization in $Fe_{52}Cr_{18}Mo_7B_{16}C_4Nb_3$ Bulk Amorphous Alloy" , Iranian Journal of Mater. Sci. Eng., Vol. 7, Number 4, 2010, 25-29.

[DOI: 10.22068/ijmse.12.2.83]